https://doi.org/10.5194/essd-2023-107
Preprint. Discussion started: 5 April 2023

Open Access Earth System Science Data Discussions

GEST: A multi-scale dynamics-based reconstruction of global ocean surface current

Guiyu Wang [1], Ge Chen [1], Chuanchuan Cao [1], Xiaoyan Chen [1], and Baoxiang Huang [2]

[1]Frontiers Science Center for Deep Ocean Multispheres and Earth System, School of Marine Technology, Ocean University of China, Qingdao, China

[2]Department of Computer Science and Technology, College of Computer Science and Technology, Qingdao University, Qingdao, China

Corresponding to: G.Y. Wang (guiyuwang@stu.ouc.edu.cn)

Abstract A high precision and fine resolution reconstruction of sea surface current is beneficial to the exploration of complicated ocean dynamic processes. Existing studies mainly use satellite sea level and wind stress fields to derive sea surface geostrophic and Ekman currents, and build physical inversion models for global or regional oceans. Despite the obvious success, there are a variety of typical dynamic processes in the ocean such as mesoscale eddies and small-scale waves, and any product of surface current that neglects the contribution of wave motion would be, at best, incomplete. In this context, we present a precise sea surface current product at 15 m depth named GEST (Geostrophic-Ekman-Stokes-Tide) by analyzing the coupling relationship between ocean surface components that correspond to different physical processes and the actual currents as observed by drifting buoys. The GEST was generated based on Ekman, geostrophic currents, and waved-induced Stokes drift and TPXO9 tidal currents. Specifically, in the calculation of Ekman currents, local applicability is taken into account to ensure that the friction layer of wind-driven current can reach where drifters could operate as normal. A comparison proves that combining multi-scale theory and the condition of local applicability improves estimation results by up to 3.6 cm/s compared with OSCAR product, and 0.3 cm/s with GlobCurrent. Furthermore, by comparing the reconstructed products with 1° and 0.25° resolution, we find that the higher resolution not only reveals more details of ocean currents especially mesoscale eddy energy associated with geostrophic currents, but also improves the accuracy by up to 5.62 cm/s.

https://doi.org/10.5194/essd-2023-107
Preprint. Discussion started: 5 April 2023

1 Introduction

The ocean surface current is fundamental for climate studies and is closely associated with many oceanographic applications (Lagerloef et al., 2003; Caniaux et al., 2005; Jin et al., 2014). Detailed information of these currents significantly affects fisheries management, shipping control and ocean rescue (Lo et al., 1998). In particular, the knowledge of velocities and directions of ocean surface current is necessary for the tracking of suspended matter (such as spilled oil, algae, sea ice, and floating microplastic) (Choi et al., 2013; Yang et al., 2014; Weisberg et al., 2019; Onink et al., 2019), which can effectively explore plankton ecology and safeguard marine ecology (Wahl et al., 1996; Garçon et al., 2001). Therefore, high-resolution, long time series of ocean surface current are needed to extend existing oceanographic datasets, deepen the understanding of refined ocean dynamic processes, and make accurate predictions about changes in the climate system (Chapman et al., 2017).

Emerging technologies have been effectively applied to the observation of ocean surface current, but there is no global current observation system to obtain sea surface velocities on a full spatial and temporal scale so far. Despite the obvious success of the Global Drifter Program (GDP) issued by the National Oceanic and Atmospheric Administration (NOAA) which has run for about 40 years, limitations and shortcomings like coarse space-time sampling and few coastal distributions are also existing.

It is well understood that satellite-based algorithms can explain about 70 % of the global ocean current dynamics (Sudre and Morrow, 2008), in which large-scale geostrophic circulation has been determined over the last 25-30 years. When forming a steady balance between wind-induced frictional stresses and Coriolis forces, Ekman current is the theoretical basis for understanding wind-driven ocean component, and is similarly considered as another main dynamic mechanism of ocean currents (Ekman, 1905). Remarkable progress has been made in estimating long time series ocean surface current datasets following the construction of global physical estimation model, such as the OSCAR (Ocean Surface Current Analysis Real Time), GEKCO (Geostrophic and Ekman Current Observatory) and the GlobCurrent project (Bonjean and Lagerloef, 2002; Dohan and Maximenko, 2010; Sudre et al., 2013; Rio et al., 2014). Sudre et al. (2013) obtained wind-driven currents by reanalyzing wind stress fields based on a two-parameter model, in which parameters were modified by linear stability equations based on the assimilation of drifter data.

https://doi.org/10.5194/essd-2023-107
Preprint. Discussion started: 5 April 2023

The global geostrophic component was determined from the gradients ($\partial h/\partial y$, $\partial h/\partial x$) of the ocean sea surface height (SSH), which was calculated from the sum of the altimeter sea-level anomaly (SLA) and the mean dynamic topography (MDT). In the equator, a β-plane geostrophic approximation proposed by Lagerloef et al. (1999) was adopted because of the vanishing of the Coriolis force. Rio et al. (2014) used a new 0.25° CNES-CLS13 MDT by assimilating drifter observations, with which the velocities in strong currents were increased by 200 % on average. In addition, they also calculated a two-level (0 m and 15 m) empirical Ekman model with surface drifters and Argo floats, and both piece of algorithms lead to more accurate ocean currents. Bonjean and Lagerloef (2002) gained the improved estimate of tropical circulation with geostrophic, Ekman, Stommel shear dynamics, and a complementary term from surface buoyancy gradient, with quasi-linear and steady physics. All these surface currents were directly calculated from geostrophic and wind-induced Ekman currents. In the actual ocean, however, the movement of upper oceans is the result of multiple environmental driving mechanisms, and can be broadly divided into large-scale ocean circulations, micro scale internal waves and storm surges. Wave-induced transport acts either as an enhancement or attenuation to the mean flow within Ekman layer, and should also be regarded as an essential source of the ocean current (Bi et al., 2012).

In this paper, we examine the inherent coupling relationship between velocities measured by drifters and components of ocean surface current, including geostrophic and Ekman currents, wave-induced tidal currents and Stokes drift, which results in a more accurate ocean surface current product incorporating multi-scale dynamic mechanisms. This global daily product covers the period of 2013-2019, with a 0.25° spatial resolution, and is compared with the OSCAR product and the GlobCurrent project.

The organization of the remaining parts of this paper is as follows. Section 2 is concerned with the data used to calculate the components of the flow field. Section 3 presents the method to reconstruct ocean surface current. Section 4 shows the results of flow field estimates and provides a discussion of our estimation work. Finally, we reveal the conclusions in Sect. 5.

2 Data

2.1 Tidal data

Recently, many tidal estimation models with different resolutions and precision have emerged

https://doi.org/10.5194/essd-2023-107
Preprint. Discussion started: 5 April 2023

because of insufficient tidal observation stations (e.g., HAMTIDE, FES, and TPXO) (Lyard et al., 2006; Taguchi et al., 2014). We use the tidal data from the latest version of TPXO models available at the time of the study, the TPXO9 model, which is based on the two-dimensional positive pressure fluid equation, applying the generalized inversion method to assimilate altimetry data (e.g., satellite altimetry from T/P, ERS1, 2, Envisat satellites) and in situ station-based tidal data, and then fitting the data with the least squares (LS) (Egbert et al., 2002; Egbert et al., 2018).

Established by Gary Egbert and Lanna Erofeeva from Oregon State University, USA, the TPXO9-atlas we used for the global hourly tidal data set has accurate and reliable results, which is reflected in the low root mean square error of M2 constituents in the deep ocean, the shallow sea, and the continental shelf (Sun et al., 2022). The derived tidal data has a 1/6° resolution and contains the harmonic constant of 15 constituents, including eight major constituents (M2, S2, N2, K2, K1, O1, P1, and Q1).

2.2 Wind data

The global daily wind fields we used were retrieved from QuikSCAT and Windsat satellites launched by the United States during in-orbit operation, with a cell size of 0.25°× 0.25°, spanning 14 years from January 2006 to January 2019. This data sets were then used to calculate wind stress fields by a bulk formula, which refers to a drag coefficient (C_d) that curve-fits data for low-to-moderate winds with data for high wind speeds (Oey et al., 2006).

Based on the reanalysis wind stress fields, we aim to obtain wind-induced Ekman currents, which are perpendicular and shifted to the left of the direction of wind stress in the southern hemisphere (the opposite in the Northern Hemisphere), forming a spiral in response to the turbulent viscosity that depends on the local ocean state (Roach et al., 2015).

2.3 CMEMS global geostrophic currents and Stokes drift

The reanalysis daily geostrophic velocities generated by Copernicus Marine Environment Monitoring Service (CMEMS) with a grid size of (0.25)°× (0.25)° are used in this study (Pujol et al., 2016) covering the years 2006-2019. For latitudes outside ±5° N, geostrophic currents are obtained from altimeter maps of the Absolute Dynamic Topography (ADT) using a nine-point stencil width methodology. While near the equatorial zone, the geostrophic balance is not applicable anymore and a β-plane approximation of Lagerloef et al. (1999) is introduced.

https://doi.org/10.5194/essd-2023-107
Preprint. Discussion started: 5 April 2023

In addition, the Stokes drift is taken from the Global Ocean Waves Reanalysis (WAVERYS) numerical assimilation products of CMEMS at grid points with 0.2° longitude and 0.2° latitude spacing covering the years 2006 to 2019. These products involve 3-hour instantaneous fields of integrated wave parameters (e.g., Sea surface wave significant height (SWH), sea surface wind wave from direction (WW), and Stokes drift velocities (VSDXY)), and are derived from the global wave reanalysis of the MeteoFranceWAve-Model (MFWAM) wave model by assimilating the altimeter wave data and directional spectrum provided by Sentinel-1 (Law-Chune et al., 2021).

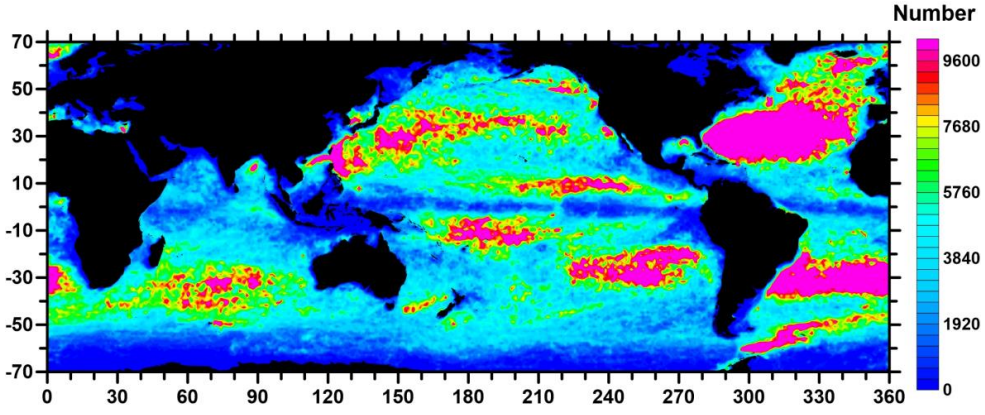

Figure 1: Spatial distribution for the drifter observations per 1° × 1° from 1999 to 2019.

2.4 Surface drifting buoys

AOML's Global Drift Program consists of a global array of more than 1,000 satellite-tracked surface drifting buoys ("drifters") that take large scale measurements of surface velocities and track the direction of currents by Lagrangian method. In this study, we use the velocities of these in situ drifters as 'reference tags'. This global data set with long time series is interpolated at hourly intervals and contains rich details of global high-frequency and small-scale ocean processes. Positions and velocities are derived by locally modelling the trajectories to construct first-order polynomials, whose coefficients are obtained by maximizing the likelihood function (Elipot et al., 2016; Elipot et al., 2022). To give an idea about the collocated drifter data set, the global spatial distribution of the drifter observations per 1°×1° cell is shown in Fig. 1.

3 Reconstruction of sea surface current at 15 m depth

https://doi.org/10.5194/essd-2023-107
Preprint. Discussion started: 5 April 2023

3.1 Local applicability of wind-driven currents

We use the two-parameter empirical model displayed in Eq. (1) to estimate Ekman Currents ($\boldsymbol{u_e}$,$\boldsymbol{v_e}$) (Niiler and Paduan, 1995; Sudre and Morrow, 2008),

$$(\boldsymbol{u_e} + \boldsymbol{iv_e}) = Be^{i\theta}\left(\boldsymbol{\tau_x} + \boldsymbol{i\tau_y}\right), \quad (1)$$

where τ_x and τ_y represent zonal and meridional wind stress. In the region out of 25° S-25° N, we follow the amplitude B = 0.3 m s^{-1} pa^{-1} and the vectoring angle θ = 55° with respect to the wind stress direction. Near the equator (25° S-25° N), the latitude-dependent parameters B and θ derived by Lagerloef et al. (1999) are adopted which are related to the Coriolis force parameter f, the water density ρ= 1025 kg m^{-3}, the linear drag coefficient r_e = 2.15×10^{-4} m s^{-1}, and the friction depth (h_e=32.5 m),

$$B = \frac{1}{\rho}\left({r_e}^2 + f^2{h_e}^2\right)^{-\frac{1}{2}} \quad (2a)$$

$$\theta = \arctan\left(\frac{fh_e}{r_e}\right). \quad (2b)$$

A climatological annual mean of Ekman currents as well as the geostrophic, Stokes, and tidal components is shown in Fig. 2. It seems that the uncertain assessment scheme of parameters (B and θ) within equatorial band proposed by Lagerloef et al. (1999) leads to high Ekman current velocities, which contradicts the theory of calm belt near the equator. Although previous studies have calibrated parameters (B, θ) by using the least squares fit based on ageostrophic wind-driven velocities obtained by subtracting geostrophic component from the drifting buoy velocities, it does not constitute a fully independent validation with our reference field in this study. Accurate and independent parameter scheme of wind-driven velocities may be an improvement of this work in the future.

Subject to wind stress intensity and the viscosity coefficient of seawater, the friction depth of wind-driven currents (or Ekman depth) is locally adaptive, ranging from a few meters to hundred meters. A verification is necessary that the mixing depth of the Ekman layer reaches the position of the drogued drifters. Following a linear steady momentum balance in Eq. (3a) and Eq. (3b) proposed

https://doi.org/10.5194/essd-2023-107
Preprint. Discussion started: 5 April 2023

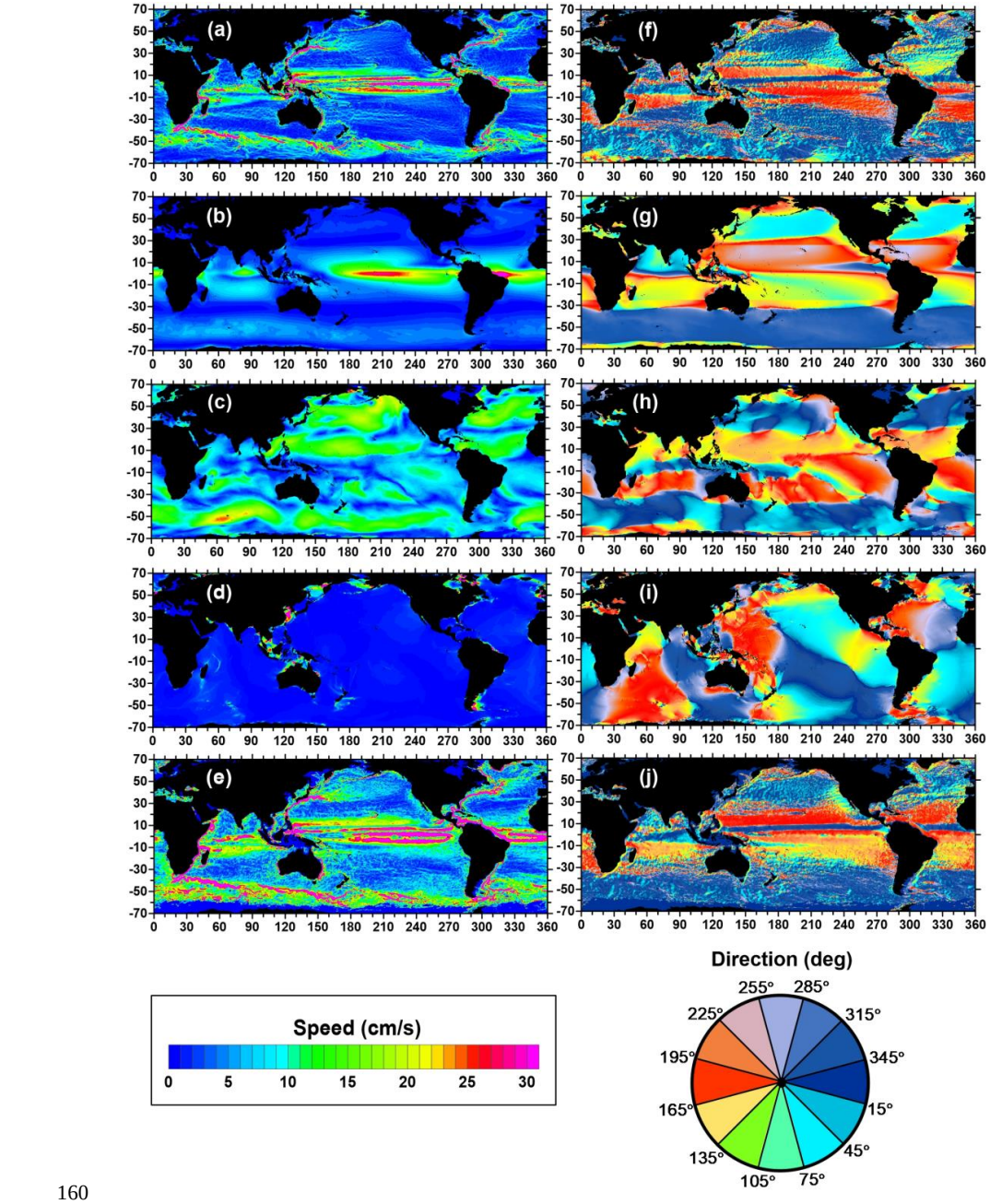

Figure 2: Global annual climatological flow fields. The left column represents flow speed of (a) geostrophic currents for 1999-2019, (b) Ekman currents for 1999-2019, (c) Stokes drift for 2013-2019, (d) tidal currents for 2013-2019, and (e) drifter observations for 1999-2019. While the right column is the flow direction.

https://doi.org/10.5194/essd-2023-107
Preprint. Discussion started: 5 April 2023

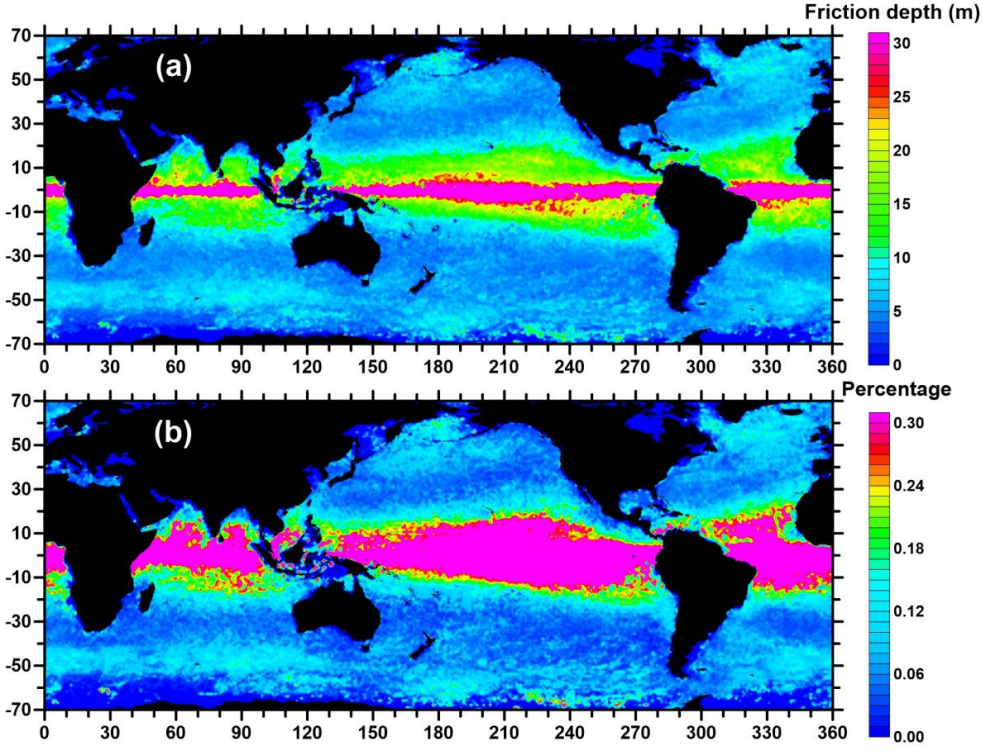

Figure 3: (a) Global mean distribution of the friction depth per 1° × 1°. (b) Proportion of friction depth up to 15 m in drifter observations.

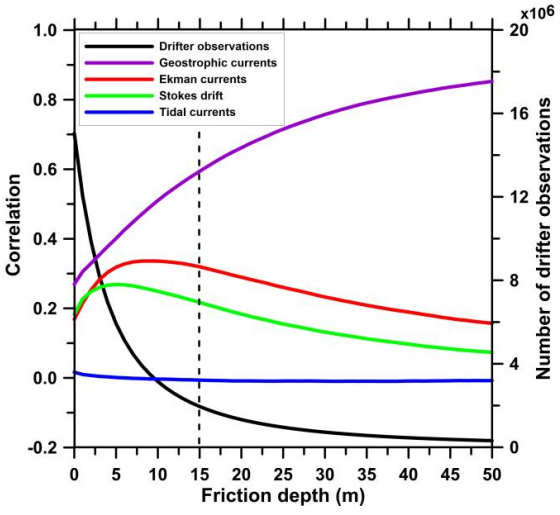

Figure 4: The correlation between four flow fields and observed velocity of drifters (left axis), and the number of drifter observations varying with Ekman depth h_e (right axis).

https://doi.org/10.5194/essd-2023-107
Preprint. Discussion started: 5 April 2023

by Meurs and Niiler (1997) and Lagerloef et al. (1999), the friction depth h_e of Ekman currents can be expressed by Eq. (3c),

$$f h_e \boldsymbol{u} + r_e \boldsymbol{v} = \boldsymbol{\tau_y}/\rho \tag{3a}$$

$$r_e \boldsymbol{u} - f h_e \boldsymbol{v} = \boldsymbol{\tau_x}/\rho \tag{3b}$$

$$h_e = \frac{1}{f} \frac{\boldsymbol{\tau_y u} - \boldsymbol{\tau_x v}}{\rho\,(\boldsymbol{u}^2 + \boldsymbol{v}^2)}\,, \tag{3c}$$

where u and v are ageostrophic vectors when removing geostrophic velocities from drifters observations of monthly climate state. Figure 3a illustrates a global climatological distribution of Ekman depth per 1° grid. With the deepening of Ekman depth h_e, the correlation between currents components and drifter velocities shows a trend of increase and then decrease, with the latter possibly related to the sharp decline in the number of drifter observations after the validation of wind-driven friction depth (Fig. 4). We select 15 m friction depth as the minimum threshold for

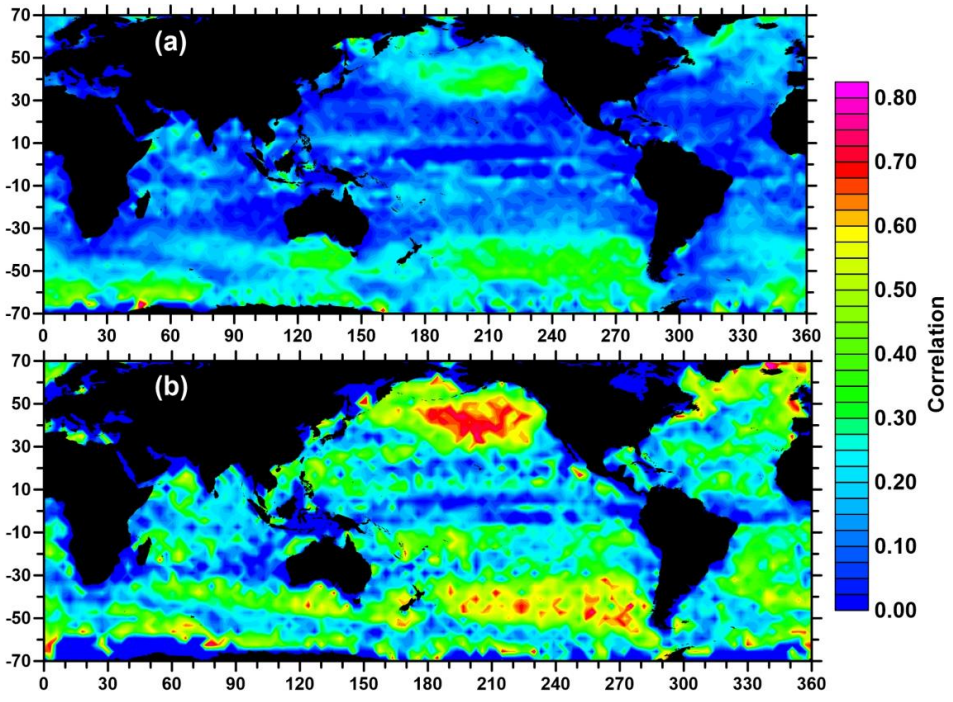

Figure 5: The correlation between Ekman currents and drifter observations per 3° grid (a) before and (b) after depth validation.

https://doi.org/10.5194/essd-2023-107
Preprint. Discussion started: 5 April 2023

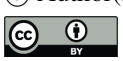

the filtration of Ekman currents datasets by comprehensively considering the location of drogued drifters, the correlation between ocean components and drifter observations, and the change in the number of drifter observations. The ratio of drifter observations filtered by the selected friction depth (15 m) to all drifter observations indicates that about 9/10 of the quantities have been culled (Fig. 3b). Figures 5a and 5b show that the correlation between Ekman currents and drifter observations increases by ~15 % after the filtration.

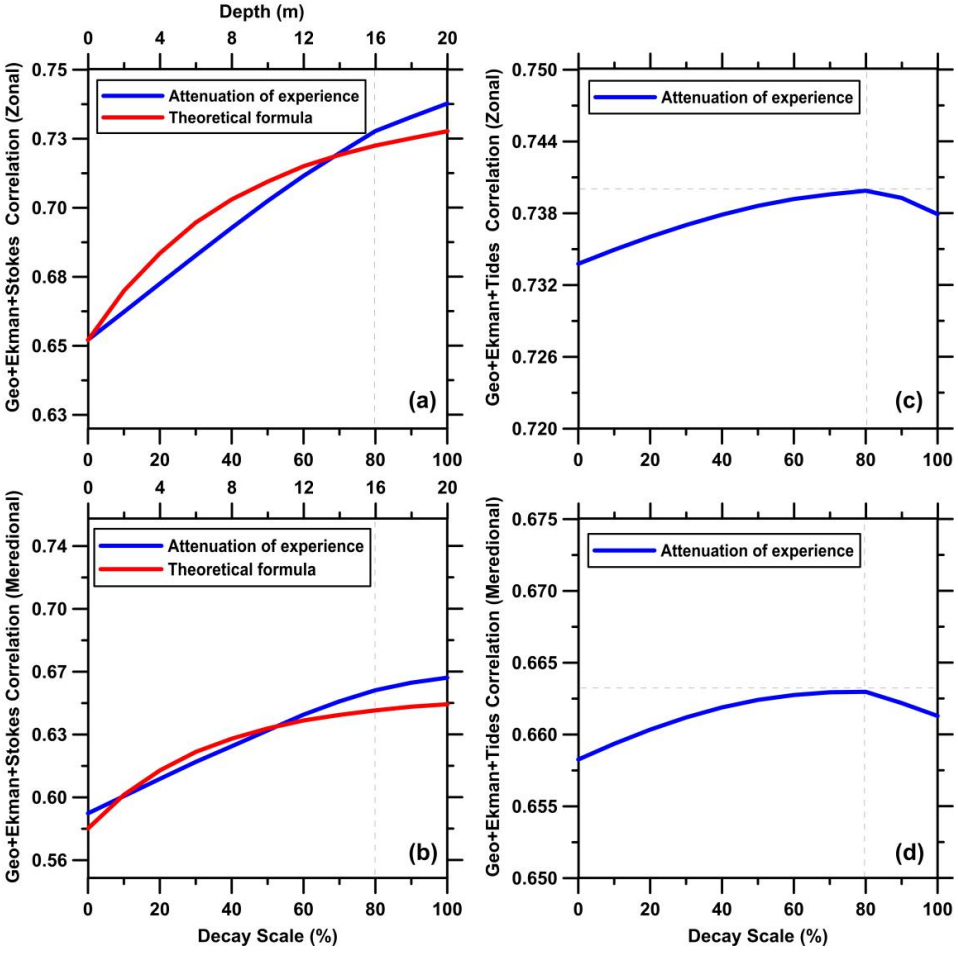

Figure 6: The correlation of the zonal (top) and meridional (bottom) vector combinations of (a)-(b) geostrophic, Ekman currents, and Stokes drift, decaying with depth (top coordinate) and percentage (bottom coordinate), and (c)-(d) geostrophic, Ekman currents, and tidal currents decaying with percentage.

https://doi.org/10.5194/essd-2023-107
Preprint. Discussion started: 5 April 2023

196 3.2 Decay scales of Stokes drift and tidal currents

197 The reanalysis Stokes drift and tidal currents cover 0 m vertically and need to be attenuated by
198 empirical percentage method and exponential method that can be expressed in Eq. (4),

199 $$\boldsymbol{u_s} = \boldsymbol{u_{s0}} \exp(2kz), \quad (4)$$

200 where u_{s0} denotes the surface Stokes drift, z is the profile derived from a monochromatic wave
201 with wavenumber k and wavelength (Kukulka and Harcourt, 2017). As shown in Figs. 6a-6d, the
202 correlation between drifter observations and different vector combinations of geostrophic, Ekman,
203 tidal currents, and Stokes drift, increases ceaselessly with depth when using the theoretical formula
204 and, for tides, reaches peaks at 80 % attenuation when adopting the percentage decay method.
205 Thus, the 80 % decay ratio is used for Stokes drift and tidal currents before the subsequent
206 estimation of surface current.

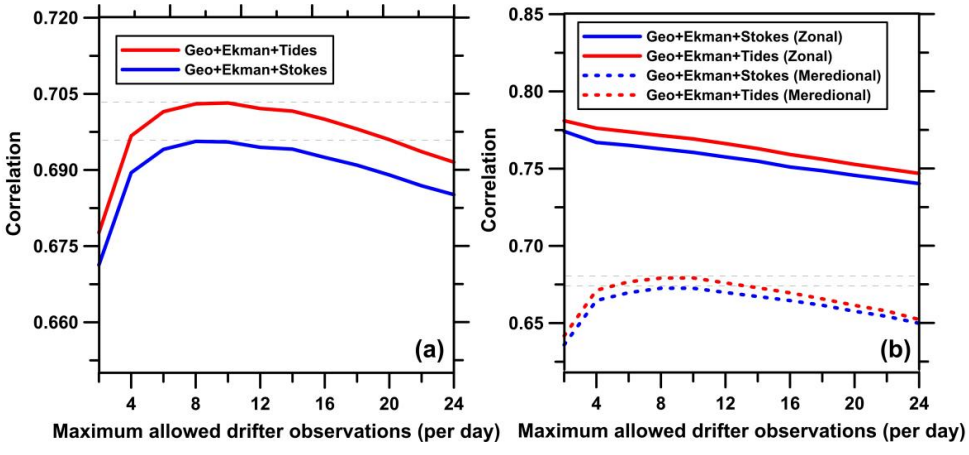

207

208 **Figure 7:** The correlation of different combinations of geostrophic, Ekman, tidal currents, and
209 Stokes drift varying with maximum allowed drifter observations per day corresponding to (a)
210 vector synthesis and (b) zonal and meridional vector.

211 3.3 Optimal time matching interval between wind fields and drifter observations

212 Exact correspondence matching with the retrieved time of wind field will result in insufficient drift

https://doi.org/10.5194/essd-2023-107
Preprint. Discussion started: 5 April 2023

observations. Based on a series of experiments, we confirm that the correlation between synthesized vectors or their components of geostrophic, Ekman, tidal currents, and Stokes drift (Figs. 7a and 7b) and the maximum allowed drifter observations per day peaks near the number of 12 (i.e., the time interval is no more than 6 hours).

3.4 Correlation analysis of ocean current components with drifter observations

A new drifter data set has been constructed by matching the pre-processed geostrophic currents, Ekman currents, Stokes drift and tidal currents. We then reveal the coefficient of the Pearson correlation between ocean components and drifter observations referring to Eq. (5) which is related to true observations (x_i, y_i) and the averaged ones $(\overline{x}, \overline{y})$,

$$Pearson = \frac{\sum_{i-1}^{n} (x_i - \overline{x})(y_i - \overline{y})}{\sqrt{\sum_{i=1}^{n} (x_i - \overline{x})^2} \sqrt{\sum_{i=1}^{n} (y_i - \overline{y})^2}}. \quad (5)$$

Going through Figs. 8a-8d, the contribution of each component to the flow field is clearly evident. Geostrophic currents act as the primary mechanism that form the ocean surface current field, and the Pearson correlation coefficient can reach nearly 0.98 in the regions with strong and persistent

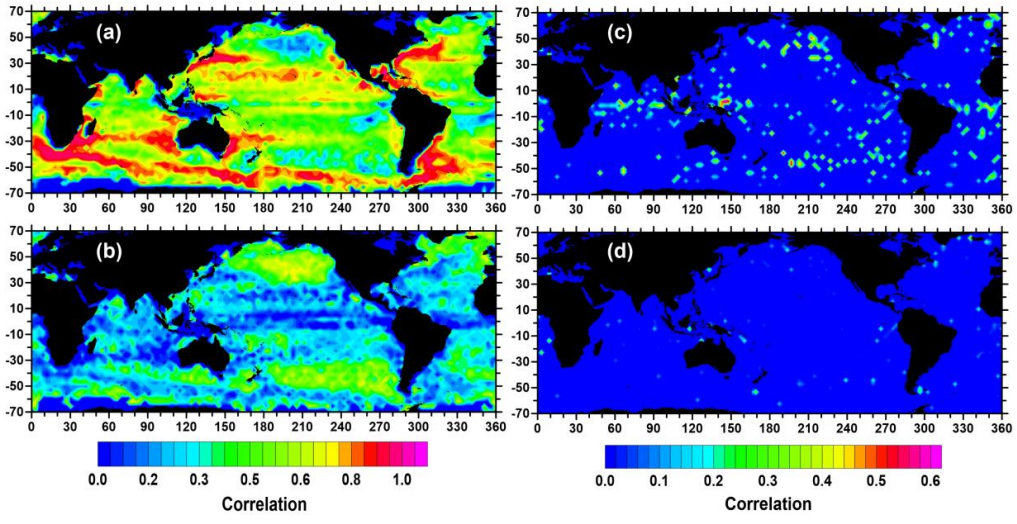

Figure 8: Geographical distribution of the Pearson correlation coefficient of (a) geostrophic currents, (b) Ekman currents, (c) Stokes drift, and (d) tidal currents.

https://doi.org/10.5194/essd-2023-107
Preprint. Discussion started: 5 April 2023

currents along the western boundary. Moreover, wind-induced Ekman currents contribute significantly in the westerly zone of the northern and southern hemispheres, while are not noticeable near the equator, which may be related to the calm zone in the tropics. At the same time, Stokes drift can contribute up to 60 % in the West Pacific, while tidal currents work mainly in the shallow coastal area with the maximum value of 0.5, which is consistent with its higher velocities along the coast.

3.5 Optimal GEST model for estimating ocean surface current

Given the seasonal and local variability in velocity and direction of the surface current, we first build least-squares linear regression (Eq. (6)) on a 3° grid by season using different flow field combinations (Sub-GE (Geostrophic-Ekman), Sub-GES (Geostrophic-Ekman-Stokes), Sub-GET (Geostrophic-Ekman-Tide), and Sub-GEST (Geostrophic-Ekman-Stokes-Tide)) to determine the optimal configuration of the flow field components,

$$E = \sum_{i=0}^{n} {e_i}^2 = \sum_{i=1}^{n} (y_i - \hat{y}_i)^2 , \quad (6)$$

where $\hat{y_i}$ is the predicted observation, y_i is the true ones, and n is the number of observations. Four initial datasets, called GEST-1, were obtained based on the sub-models above (Sub-GE, Sub-GES, Sub-GET, Sub-GEST) by using the data from 2006-2012. We verified the error of the GEST-1 versus drifter data with root mean square error (RMSE),

$$RMSE = \sqrt{\frac{1}{n}\sum_{n=1}^{n} (\hat{y}_i - y_i)^2} . \quad (7)$$

Table 1 shows a regional comparison regarding the reconstruction errors of the sub-models. In the Antarctic Circumpolar Current (ACC) where the GE model has a higher accuracy, it seems that the inclusion of tidal currents and Stokes drift contributes to signal noise, while in the equatorial regions of Pacific and Indian Ocean, the results of the Sub-GEST are significantly better than other combinations. In addition, compared with Sub-GE model (Figs. 9a and 9b), the Sub-GES is more effective mainly in the western equatorial Pacific, such as the Peninsular Malaysia and Marshall Islands (Figs. 9e and 9f). Furthermore, as shown in Figs. 9g and 9h, the averaged RMSE of Sub-

https://doi.org/10.5194/essd-2023-107
Preprint. Discussion started: 5 April 2023

254 GET in the south coast of Kyushu Island decreased to 11.35 cm/s from about 11.75 cm/s of the
255 Sub-GE (Fig. 9c), and the Gulf of Mexico also decreased about 0.3 cm/s than Sub-GE (Fig. 9d)
256 with a maximum decrease of up to 10 % in this region, which is likely related to frequent tropical

257 **Table 1.** Verified RMSE (cm/s) based on Sub-GE/ Sub-GES/ Sub-GET/ Sub-GEST models

Reconstruction Model	Longitude and Latitude			
	55° E-70° E 10° S-5° N	80° E-100° E 45° S-60° S	103° E-113° E 3° N-19° N	125° E-142° E 22° N-37° N
Sub-GE	22.0333	9.1091	12.3418	11.7525
Sub-GES	20.9319	9.2731	11.9773	11.9136
Sub-GET	23.3724	9.2368	12.4657	11.3579
Sub-GEST	20.6216	9.3872	12.0061	11.4845
Reconstruction Model	Longitude and Latitude			
	156° E-173° E 10° S-10° N	175° E-195° E 40° S-55° S	228° E-240° E 9° S-21° S	260° E-290° E 18° N-28° N
Sub-GE	16.9963	7.1911	6.5527	7.9553
Sub-GES	16.4886	7.3135	6.5541	8.0693
Sub-GET	17.0196	7.2609	6.5225	7.6361
Sub-GEST	16.5005	7.3945	6.5184	7.8609

258 cyclone activities in the Gulf of Mexico and the southern coast of Kyushu Island. From August to
259 October, the South Kyushu Island is vulnerable to tropical cyclones in the Northwest Pacific Ocean,
260 while storm surges in the north dominate in the Gulf of Mexico. Driven by typhoons, seawater

https://doi.org/10.5194/essd-2023-107
Preprint. Discussion started: 5 April 2023

rises steeply to form storm surges, with water levels sometimes reaching 5 m. When storm surges are superimposed on astronomical surges, the magnitude of water level changes could be even greater (Murty et al., 1986; Dube et al., 1997; Bilskie et al., 2016).

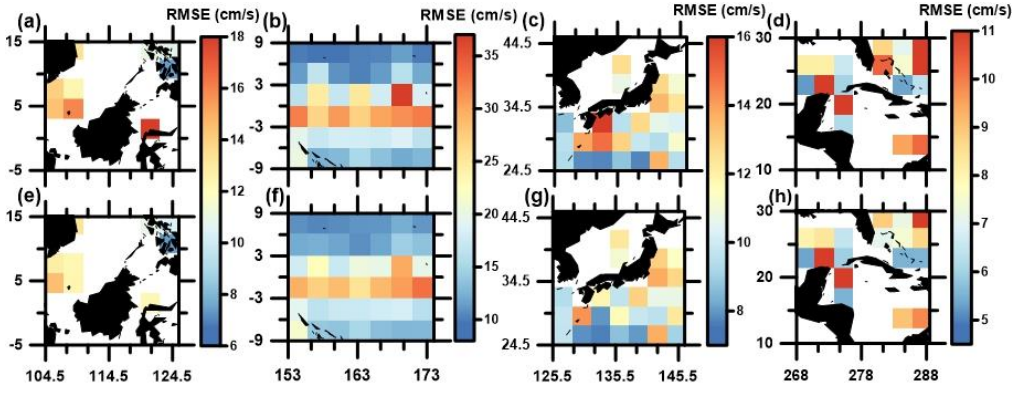

Figure 9: RMSE of (a)-(d) Sub-GE, (e)-(f) Sub-GES, and (g)-(h) Sub-GET models.

As mentioned above, wave-induced Stokes drift and tidal currents contribute significantly only in certain regions (see Table 1) and should not be joined entirely on a global scale. Thus, the optimal GEST model was chosen from the above sub-models (Sub-GE, Sub-GES, Sub-GET, and Sub-GEST) per 3° × 3° grid by the error validation of the regression, and then was used for the estimates of ocean surface current incorporating geostrophic and Ekman currents, Stokes drift, and tidal currents.

4 Result and discussion

4.1 GEST products and associated verification

Following the optimized reconstruction scheme outlined above, a 0.25° resolution data set named GEST, such as the daily current velocity on a particular reference date (Fig. 10), was obtained combining the geostrophic flow with other field components. We have also considered building products with 1° resolution by matching other flow fields with Ekman currents, but quantitative validations showed that the 0.25° reconstructed field significantly decreased global averaged RMSE from about 14.61 cm/s to 9.36 cm/s over the 1° resolution product. Figures. 11a-11c show

https://doi.org/10.5194/essd-2023-107
Preprint. Discussion started: 5 April 2023

the global distribution of the RMSE for 1° product, with significant errors in the western boundary currents and the Kuroshio area. It appears that intense kinetic energies of mesoscale eddies exist in these regions (Fig. 12) and likely neglected by the coarse spatial resolution (Chen and Han, 2019).

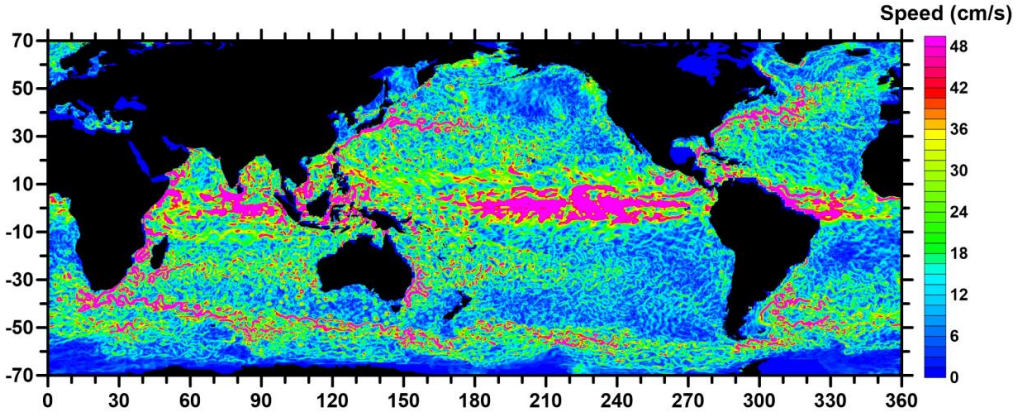

Figure 10: Daily current field of the GEST product on 01 January 2017.

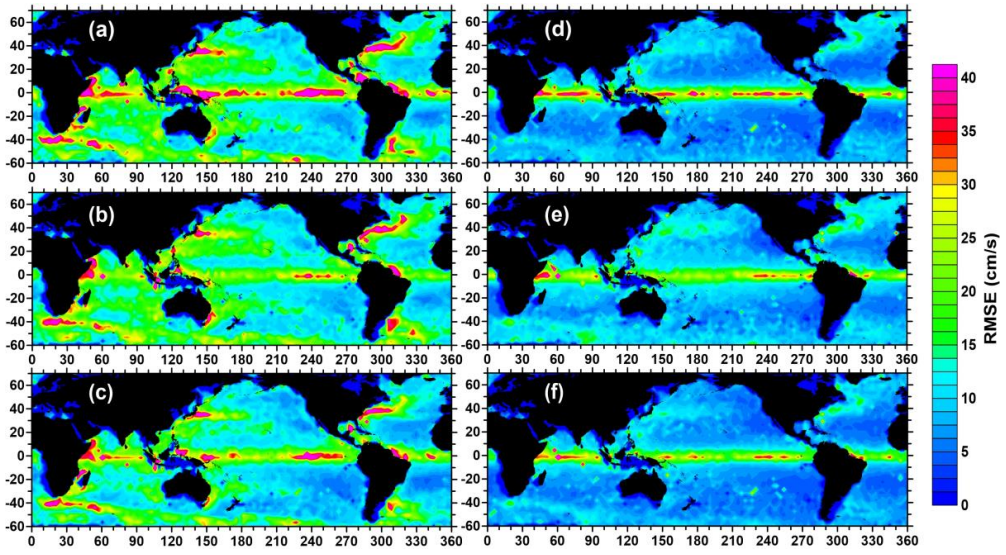

Figure 11: The RMSE of the 1° reconstructed field of (a) zonal vector, (b) meridional vector, and (c) synthetic vector, and the 0.25° reconstructed field of (d) zonal vector, (e) meridional vector, and (f) synthetic vector with the optimal GEST model.

https://doi.org/10.5194/essd-2023-107
Preprint. Discussion started: 5 April 2023

290 Moreover, compared with the estimates of regression theory, we find that the optimal vector
291 synthesis scheme has a higher reconstruction accuracy in estimating the 0.25° resolution field, and
292 additionally, traditional geostrophic and Ekman currents model is also available in regions without
293 reference velocities. As shown in Figs. 11d-11f, the RMSE of the optimal vector synthesis method
294 (8.99 cm/s) decreases by almost 0.4 cm/s compared with the optimal regression method (9.36 cm/s).

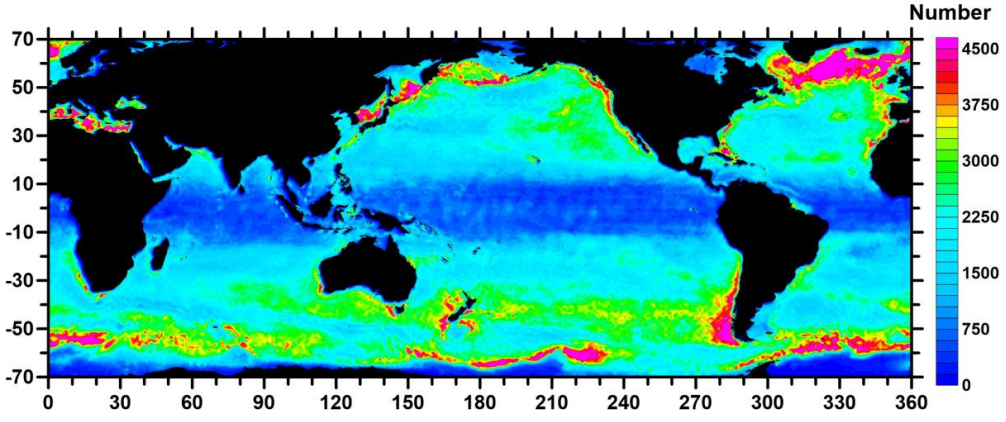

295

296 **Figure 12:** The global distribution of mesoscale eddies.

297 4.2 Comparison of the GEST to other global surface current products

298 Excellent achievements have been made in physical model-based reconstructions of ocean surface
299 current. The OSCAR near-surface current with a grid size of 1° on a 5 days basis use the quasi-
300 linear, quasi-steady sea surface momentum equations and improve the equatorial algorithm by
301 fitting 12 orthogonal polynomials (Johnson et al., 2007). Meanwhile, the GlobCurrent data set
302 presents an improved empirical Ekman model and a global 0.25° MDT by exploiting information
303 from geostrophic currents and the drogued drifters. Figures. 13a and 13c show the estimate errors
304 of the OSCAR and GlobCurrent products when compared with the velocity of the drogued drifters.
305 The RMSE of GlobCurrent is, on average, ~2 cm/s smaller than OSCAR data due to the coarse
306 temporal resolution and finite spatial distribution of T/P and Jason series altimeter data used in
307 OSCAR currents. Another promising finding is that a reduction of up to 7-8 cm/s in RMSE is
308 observed for both products when compared to drifters of which friction depths of matched Ekman
309 currents are up to 15 m (Figs. 13b and 13d).

310 In this paper, we are not able to further consider the drogue lost information because 90 % of

https://doi.org/10.5194/essd-2023-107
Preprint. Discussion started: 5 April 2023

311 drifter observations are discarded with the condition of friction layer. As evidenced in Fig. 11f, the
312 RMSE of GEST product is reduced to 8.99 cm/s compared to 12.55 cm/s for the OSCAR product,
313 and 9.28 cm/s for the GlobCurrent, and especially in the eastern equatorial Pacific, our approach
314 is quite efficient with an error reduction of up to 10 cm/s than that of OSCAR and GlobCurrent.
315 In the tropical Indian Ocean and western Pacific regions, while the GEST currents show better
316 accuracy than the GlobCurrent, the OSCAR currents outperformed both products, possibly related
317 to the improved equatorial algorithm proposed by Bonjean and Lagerloef (2002).

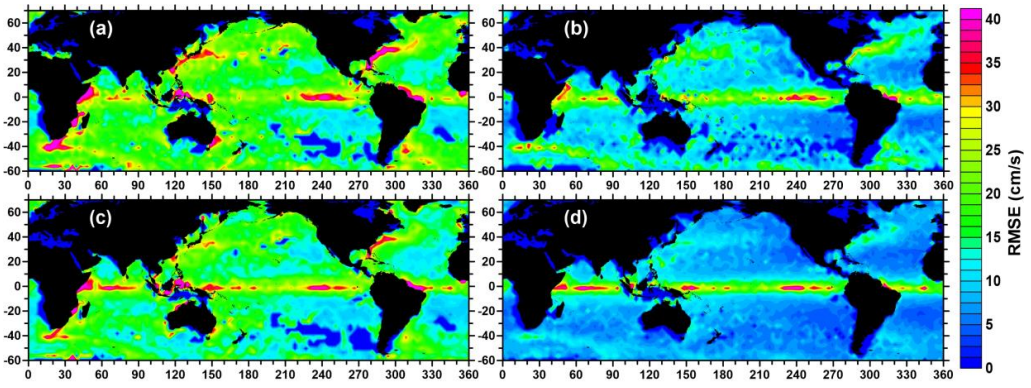

318

319 **Figure 13:** RMSE between (a) OSCAR currents and drogued drifters, (b) OSCAR currents and
320 the drifters verified by a friction depth of 15 m, (c) GlobCurrent and drogued drifters, (d)
321 GlobCurrent and the drifters verified by a friction depth of 15 m covering the years 2013-2017.

322 In addition, the reconstruction error with 1° latitudinal band was calculated for each product, as
323 well as the comparison of flow direction by radar maps, to assess the regional difference of the
324 estimation accuracy. It is quite evident that both GlobCurrent and GEST reflect better estimation
325 trends outside the equator due to the fine resolution (Fig. 14a). In particular, the GEST product
326 outperforms GlobCurrent within 60° S-50° N, which is consistent with research showing that tides
327 and Stokes drift reveal significant results in coastal and equatorial regions concentrating at low-
328 and mid-latitudes. At the equator, despite the lower spatial and temporal resolution of the OSCAR
329 data set, it also shows significant consequence with the drifter observations. Figure 14b shows that
330 GEST product has a better estimation of drifter velocity within 0°-270° angle range of the flow
331 direction than others. The lower efficiency at high latitudes and in the 270°-320° angle range is

https://doi.org/10.5194/essd-2023-107
Preprint. Discussion started: 5 April 2023

likely related to Rio et al. (2014) assimilating the drift observations used as reference fields in this paper to provide missing short-scale information in the calculation of the CNES-CLS13 MDT and wind-driven parameters with spatio-temporal variability.

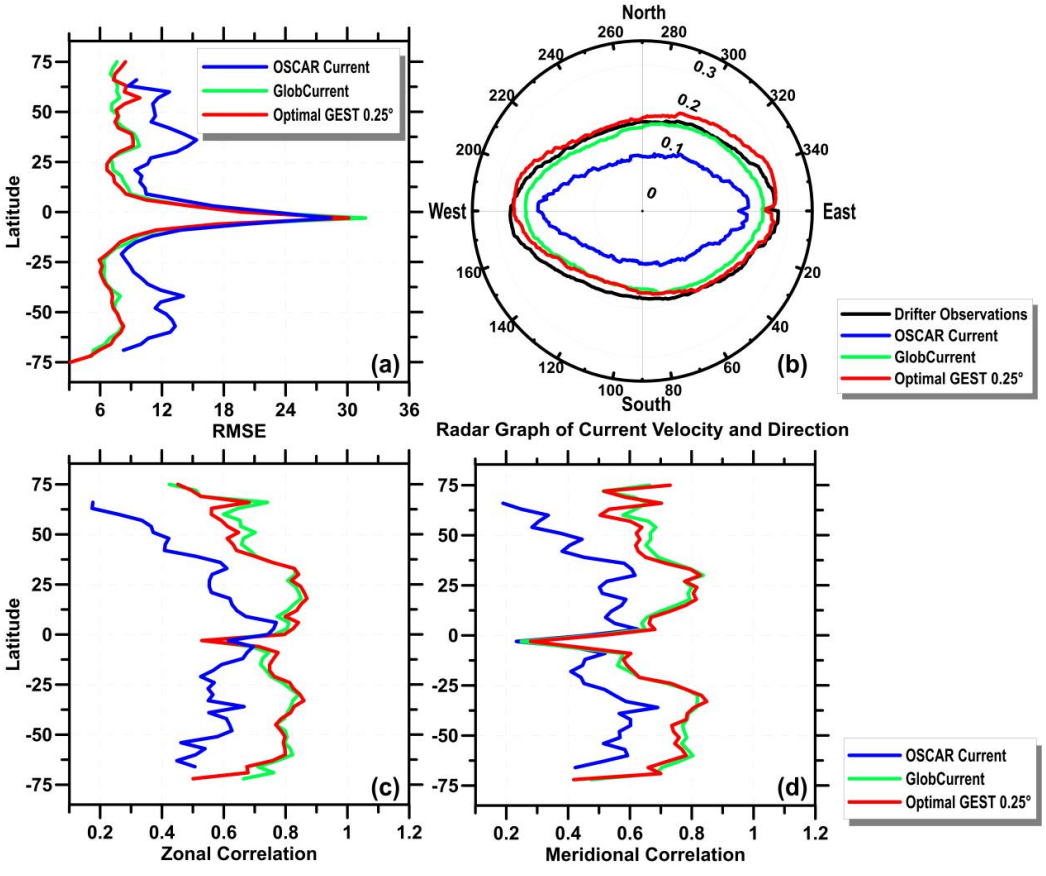

Figure 14: (a) RMSE based on latitudinal bands between each current product (the global OSCAR current (blue line), the GlobCurrent (green line), the modified 0.25° GEST current (red line)) and the surface drifters verified by a friction depth of 15 m. (b) A radar diagram of flow velocity and direction versus the drifter observations (black line), the global OSCAR current (blue line), the GlobCurrent (green line), and the modified GEST current (red line). (c) The zonal correlations and (d) the meridional correlations for the global OSCAR current (blue line), the GlobCurrent (green line), and the modified 0.25° GEST current (red line).

https://doi.org/10.5194/essd-2023-107
Preprint. Discussion started: 5 April 2023

To further verify the robustness of the results, the correlation between the ocean current products and drifter velocities in each latitudinal zone was calculated separately. As shown in Figs. 14c and 14d, the GEST product is behind GlobCurrent by about 5 % of the correlation within 40° and 55° in the Northern Hemisphere. And it, in contrast, shows higher correlation coefficients at low to mid latitudes of the Southern Hemisphere. In the equatorial region, both pieces of products remained inferior to the OSCAR data for the horizontal component, being consistent with the results of the RMSE. However, the GEST product delivers better results of meridional correlations possibly due to the addition of Stokes drift.

It is notable that existing current products have poor estimates in the equatorial within 10° S-10° N and western boundary currents. A plausible interpretation is that the parameters of wind-driven model and the higher-order balance of geostrophic velocities are still uncertain. Furthermore, previous studies have indicated that ocean eddies and large-scale planetary waves (e.g., Rossby and Kelvin waves) correspond to ocean circulation at different scales. Especially in the equatorial band, the fluctuation significantly contributes well to the upper ocean circulation. In particular, the scale of the zonal component of the eastward Kelvin wave is more significant than that of the meridional component (Forbes, 2000), which may influence the inversion accuracy of the zonal feature in the equatorial region. Meanwhile, the complex aliasing effect between intense ocean currents, eddies with strong kinetic energies, and large-scale planetary waves with strong fluctuations, is also likely to be an important factor affecting the reconstruction accuracy in this study (Hansen and Paul, 1984; Klocker and Marshall, 2014; Huang et al., 2021; Chen et al., 2022).

5 Data availability

All data used in this study are publicly available, and are listed in Table 2. The TPXO9-atlas for tidal currents is available for academic research and other non-commercial uses under previous registration from https://www.tpxo.net/global/tpxo9-atlas (Egbert et al., 2018). The GEST product produced in this research can be found at https://doi.org/10.5281/zenodo.7767202.

Table 2. Remotely sensed, in situ, and reanalysis data sets used in this paper.

https://doi.org/10.5194/essd-2023-107
Preprint. Discussion started: 5 April 2023

Data set	Link	Citation
Geostrophic current	https://data.marine.copernicus.eu/product/SEALEVEL_GLO_PHY_L4_MY_008_047/	Pujol et al. (2016)
Ocean Waves Reanalysis data	https://data.marine.copernicus.eu/product/GLOBAL_MULTIYEAR_WAV_001_032/	Law-Chune et al. (2021)
WindSat products	https://www.remss.com/missions/windsat/	Wentz et al. (2013)
Quikscat products	https://www.remss.com/missions/qscat/	Wentz et al. (2011)
Global Drifter data	https://www.aoml.noaa.gov/phod/gdp/hourly_data.php	Elipot et al. (2022)
OSCAR current	https://search.earthdata.nasa.gov/downloads/6873202440	Johnson et al. (2007)
GlobCurrent product	https://tds0.ifremer.fr/thredds/GLOBCURRENT/GLOBCURRENT.html?dataset=GLOBCURRENT-L4-CUREUL_15M-ALT_SUM-V03.0	Rio et al. (2014)

6 Concluding remarks

It is understood that there are multi-scale dynamic processes in ocean surface current, among which large-scale geostrophic circulation and wind-induced Ekman flow are widely considered, while small-scale wave phenomena are ignored. In view of the facts, a new reconstruction product of the global ocean flow field at a depth of 15 m integrating Geostrophic, Ekman, Stokes, and Tidal components is produced in this research, leading to the following conclusions:

(1) Multi-scale dynamics-based GEST product of ocean surface current is reliable because of the

https://doi.org/10.5194/essd-2023-107
Preprint. Discussion started: 5 April 2023

declining RMSE of the 0.25° resolution product which is found to be about 3.6 cm/s lower than the OSCAR product, and 0.3 cm/s lower than the GlobCurrent. In particular, the inclusion of wave-induced tidal currents and Stokes drift improves the precision of the reconstruction mainly in equatorial and coastal regions.

(2) The verification of the wind-driven friction depth with local applicability in reconstructing GEST product is significantly necessary, as evidenced by an 18 % increase in the correlation coefficient between Ekman currents and drifter velocities.

(3) It has been revealed that high-resolution product with a 0.25°×0.25° cell has a closer agreement to drifting buoys by revealing most of the mesoscale eddy kinetic energy missed by 1° resolution product and is likely to be a better indicator of the real ocean circulation given the improved accuracy of 5.62 cm/s.

It is worth pointing out that, in contrast to the existing ocean current estimation products mentioned above, better results of the proposed GEST dataset at low to mid-latitudes are obtained independently without assimilation of any drifter observation. In the future, complex mechanisms (e.g., planetary waves, eddies, etc.) will be taken into account in the equatorial and strong current regions to achieve a more accurate reconstruction of the global flow field.

Author contribution

GYW drafted the manuscript, developed the data processing, and designed the experiment. GC contributed to conceptualizing the project, supervising, reviewing and editing the paper. CCC developed the data processing and edited the paper. XYC edited and reviewed the paper. BXH supervised and reviewed the paper.

Competing interests

The authors declare that they have no conflict of interest.

Acknowledgments

The authors acknowledge that WindSat data are produced by Remote Sensing Systems and sponsored by the NASA Earth Science MEaSUREs DISCOVER Project and the NASA Earth

https://doi.org/10.5194/essd-2023-107
Preprint. Discussion started: 5 April 2023

Science Physical Oceanography Program. RSS WindSat data are available at www.remss.com. QuikScat (or SeaWinds) data are produced by Remote Sensing Systems and sponsored by the NASA Ocean Vector Winds Science Team. Data are available at www.remss.com.

This paper also acknowledges funding from the National Natural Science Foundation of China (Grant No. 42030406) and the International Research Center of Big Data for Sustainable Development Goals (No. CBAS2022GSP01).

References

Bi, F., Wu, K., and Zhang, Y.: The effect of Stokes drift on Ekman transport in the open sea. Acta Oceanol. Sin., 31(6), 12-18, https://doi.org/10.1007/s13131-012-0249-1, 2012.

Bilskie, M. V., Hagen, S. C., Alizad, K., Medeiros, S. C., Passeri, D. L., Needham, H. F., and Cox, A.: Dynamic simulation and numerical analysis of hurricane storm surge under sea level rise with geomorphologic changes along the northern Gulf of Mexico. EARTHS FUTURE, 4(5), 177-193, https://doi.org/10.1002/2015EF000347, 2016.

Bonjean, F., and Lagerloef, G. S.: Diagnostic Model and Analysis of the Surface Currents in the Tropical Pacific Ocean. J. Phys. Oceanogr., 32(10), 2938-2954, https://doi.org/10.1175/1520-0485(2002)032<2938:DMAAOT>2.0.CO;2, 2002.

Caniaux, G., Brut, A., Bourras, D., Giordani, H., Paci, A., Prieur, L., and Reverdin, G.: A 1 year sea surface heat budget in the northeastern Atlantic basin during the POMME experiment: 1. Flux estimates. J. Geophys. Res. Oceans, 110 (C7), https://doi.org/10.1029/2004JC002695, 2005.

Chapman, C., and Charantonis, A. A.: Reconstruction of subsurface velocities from satellite observations using iterative self-organizing maps. IEEE Geosci. Remote. Sens. Lett., 14(5), 617-620, https://doi.org/10.1109/LGRS.2017.2665603, 2017.

Chen, G., and Han, G.: Contrasting Short-Lived With Long-Lived Mesoscale Eddies in the Global Ocean. J. Geophys. Res. Oceans, 124(5), 3149-3167, https://doi.org/10.1029/2019JC014983, 2019.

Chen, G., Chen, X., and Cao, C.: Divergence and dispersion of global eddy propagation from satellite altimetry. J. Phys. Oceanogr., 52(4), 705-722, https://doi.org/10.1175/JPO-D-21-0122.1, 2022.

https://doi.org/10.5194/essd-2023-107
Preprint. Discussion started: 5 April 2023

Choi, J. K., Yang, H., Han, H. J., Ryu, J. H., and Park, Y. J.: Quantitative estimation of the suspended sediment movements in the coastal region using GOCI. J. Coastal Res., 65(10065), 1367-1372, https://doi.org/10.2112/SI65-231.1, 2013.

Dohan, K., and Maximenko, N.: Monitoring ocean currents with satellite sensors. OCEANOGRAPHY, 23(4), 94-103, https://doi.org/10.5670/oceanog.2010.08, 2010.

Dube, S. K., Rao, A. D., Sinha, P. C., Murty, T. S., and Bahulayan, N.: Storm surge in the Bay of Bengal and Arabian Sea: The problem and its prediction. MAUSAM, 48(2), 283-304, https://doi.org/10.54302/mausam.v48i2.4012, 1997.

Egbert, G. D., and Erofeeva, S. Y.: Efficient Inverse Modeling of Barotropic Ocean Tides. J. Atmos. Ocean. Tech., 19(2), 183-204, https://doi.org/10.1175/1520-0426(2002)019<0183:EIMOBO>2.0.CO;2, 2002.

Egbert, Y., Gary, D., and Erofeeva, S.: "TPXO9, A New Global Tidal Model in TPXO Series," in Proceedings of the Ocean Science Meeting, Portland, OR, USA: American Geophysical Union, 11–16 February 2018, 2018.

Ekman, V. W.: On the influence of the earth's rotation on ocean-currents. Ark. Mat. Asto. Fys., 2(11), 1-53, 1905.

Elipot, S., Lumpkin, R., Perez, R. C., Lilly, J. M., Early, J. J., and Sykulski, A. M.: A global surface drifter dataset at hourly resolution. J. Geophys. Res. Oceans, 121(5), 2937-2966, https://doi.org/10.1002/2016JC011716, 2016.

Elipot, S., Sykulski, A., Lumpkin, R., Centurioni, L., and Pazos, M.: Hourly location, current velocity, and temperature collected from Global Drifter Program drifters world-wide. NOAA - National Centers for Environmental Information. Dataset, https://doi.org/10.25921/x46c-3620. Accessed [13 June 2022], 2022.

Forbes, J. M.: Wave coupling between the lower and upper atmosphere: case study of an ultrafast Kelvin Wave. Journal of Atmospheric and Solar-Terrestrial Physics, 62, 1603-1621, https://doi.org/10.1016/S1364-6826(00)00115-2, 2000.

Garçon, V., Oschlies, A., Doney, S. C., McGillicuddy, D. J., and Waniek, J. J.: The role of mesoscale variability on plankton dynamics in the North Atlantic. Deep-Sea Res Pt. II, 48(10), 2199-2226, https://doi.org/10.1016/S0967-0645(00)00183-1, 2001.

Hansen, D. V., and Paul, C. A.: Genesis and effects of long waves in the equatorial Pacific. J. Geophys. Res. Oceans, 89(C6), 10431-10440, https://doi.org/10.1029/JC089iC06p10431,

https://doi.org/10.5194/essd-2023-107
Preprint. Discussion started: 5 April 2023

1984.

Huang, B., Ge, L., Chen, X., and Chen, G.: Vertical Structure-Based Classification of Oceanic Eddy Using 3-D Convolutional Neural Network. IEEE T. Geosic. Remote, 60, 1-14, https://doi.org/10.1109/TGRS.2021.3103251, 2021.

Jin, F., Boucharel, J., and Lin, I.: Eastern Pacific tropical cyclones intensified by El Niño delivery of subsurface ocean heat. Nature, 516(7529), 82-85, https://doi.org/10.1038/nature13958, 2014.

Johnson, E. S., Bonjean, F., Lagerloef, G. S., Gunn, J. T., and Mitchum, G. T.: Validation and Error Analysis of OSCAR Sea Surface Currents. J. Atmos. Ocean. Tech., 24(4), 688-701, https://doi.org/10.1175/JTECH1971.1, 2007.

Klocker, A., and Marshall, D. P.: Advection of baroclinic eddies by depth mean flow. Geophys. Res. Lett., 41(10), 3517-3521, https://doi.org/10.1002/2014GL060001, 2014.

Kukulka, T., and Harcourt, R. R.: Influence of Stokes Drift Decay Scale on Langmuir Turbulence. J. Phys. Oceanogr., 47(7), 1637-1656, https://doi.org/10.1175/JPO-D-16-0244.1, 2017.

Lagerloef, G. S., Mitchum, G. T., Lukas, R., and Niiler, P. P.: Tropical Pacific near-surface currents estimated from altimeter, wind, and drifter data. J. Geophys. Res. Oceans, 104(C10), 23313-23326, https://doi.org/10.1029/1999JC900197, 1999.

Lagerloef, G. S., Lukas, R., Bonjean, F., Gunn, J. T., Mitchum, G. T., Bourassa, M. A., and Busalacchi, A. J.: El Niño Tropical Pacific Ocean surface current and temperature evolution in 2002 and outlook for early 2003. Geophys. Res. Lett., 30(10), 1514, https://doi.org/10.1029/2003GL017096, 2003.

Law-Chune, S., Aouf, L., Dalphinet, A., Levier, B., Drillet, Y., and Drévillon, M.: WAVERYS: a CMEMS global wave reanalysis during the altimetry period. Ocean Dyn., 71(3), 357-378, https://doi.org/10.1007/s10236-020-01433-w, 2021.

Lo, H. K., and McCord, M. R.: Adaptive ship routing through stochastic ocean currents: general formulations and empirical results. Transp. Res. Part A Policy Pract., 32(7), 547-561, https://doi.org/10.1016/S0965-8564(98)00018-4, 1998.

Lyard, F. H., Lefèvre, F., Letellier, T., and Francis, O.: Modelling the global ocean tides: modern insights from FES2004. Ocean Dyn., 56(5-6), 394-415, https://doi.org/10.1007/s10236-006-0086-x, 2006.

Meurs, P. V., and Niiler, P.: Temporal Variability of the Large-Scale Geostrophic Surface Veloc-

https://doi.org/10.5194/essd-2023-107
Preprint. Discussion started: 5 April 2023

494 ity in the Northeast Pacific*. J. Phys. Oceanogr., 27(10), 2288-2297, https://doi.org/10.1175
495 /1520-0485(1997)027<2288:TVOTLS>2.0.CO;2, 1997.
496 Murty, T. S., Flather, R. A., and Henry, R. F.: The storm surge problem in the Bay of Bengal. Prog.
497 Oceanogr., 16(4), 195-233, https://doi.org/10.1016/0079-6611(86)90039-X, 1986.
498 Niiler, P. P., and Paduan, J. D.: Wind-Driven Motions in the Northeast Pacific as Measured by L-
499 agrangian Drifters. J. Phys. Oceanogr., 25(11), 2819-2830, https://doi.org/10.1175/1520-048
500 5(1995)025<2819:WDMITN>2.0.CO;2, 1995.
501 Oey, L. Y., Ezer, T., Wang, D. P., Fan, S. J., and Yin, X. Q.: Loop current warming by hurricane
502 Wilma. Geophys. Res. Lett., 33(8), 153-172, https://doi.org/10.1029/2006GL025873, 2006.
503 Onink, V., Wichmann, D., Delandmeter, P., and Van Sebille, E.: The Role of Ekman Currents,
504 Geostrophy, and Stokes Drift in the Accumulation of Floating Microplastic. J. Geophys. Res.
505 Oceans, 124(3), 1474-1490, https://doi.org/10.1029/2018JC014547, 2019.
506 Pujol, M., Faugère, Y., Taburet, G., Dupuy, S., Pelloquin, C., Ablain, M., and Picot, N.: DUACS
507 DT 2014: the new multi-mission altimeter data set reprocessed over 20 years. Ocean Sci.,
508 12(5), 1067-1090, https://doi.org/10.5194/os-12-1067-2016, 2016.
509 Rio M. H., Mulet, S., and Picot. N.: Beyond GOCE for the ocean circulation estimate: Synergetic
510 use of altimetry, gravimetry, and in situ data provides new insight into geostrophic and Ek-
511 man currents. Geophys. Res. Lett., 41(24), 8918-8925, https://doi.org/10.1002/2014GL0617
512 73, 2014.
513 Roach, C. J., Phillips, H. E., Bindoff, N. L., and Rintoul, S. R.: Detecting and Characterizing
514 Ekman Currents in the Southern Ocean. J. Phys. Oceanogr., 45(5), 1205-1223,
515 https://doi.org/10.1175/JPO-D-14-0115.1, 2015.
516 Sudre, J., and Morrow, R. A.: Global surface currents: a high-resolution product for investigating
517 ocean dynamics. Ocean Dyn., 58(2), 101-118, https://doi.org/10.1007/s10236-008-0134-9,
518 2008.
519 Sudre, J., Maes, C., and Garçon, V.: On the global estimates of geostrophic and Ekman surface
520 currents. Limnol. Oceanogr. Methods, 3(1), 1-20, https://doi.org/10.1215/21573689-2071927,
521 2013.
522 Sun, W., Zhou, X., Zhou, D., and Sun, Y.: Advances and Accuracy Assessment of Ocean Tide M
523 -odels in the Antarctic Ocean. Front. Earth Sci., 10, https://doi.org/10.3389/feart.2022.7578
524 21, 2022.

https://doi.org/10.5194/essd-2023-107
Preprint. Discussion started: 5 April 2023

525 Taguchi, E., Stammer, D., and Zahel, W.: Inferring deep ocean tidal energy dissipation from the
526 global high-resolution data-assimilative HAMTIDE model. J. Geophys. Res. Oceans, 119(7),
527 4573-4592, https://doi.org/10.1002/2013JC009766, 2014.
528 Wahl, T., Skoḙlv, A., Pedersen, J. P., Seljelv, L. G., Andersen, J. H., Follum, O. A., Anderssen,
529 T., Strøm, G. D., Bern, T. I., Espedal, H. H., Hamnes, H., and Solberg, R.: Radar satellites:
530 A new tool for pollution monitoring in coastal waters. Coast. Manage., 24(1), 61-71,
531 https://doi.org/10.1080/08920759609362281, 1996.
532 Weisberg, R. H., Liu, Y., Lembke, C., Hu, C., Hubbard, K., and Garrett, M.: The Coastal Ocean
533 Circulation Influence on the 2018 West Florida Shelf K. brevis Red Tide Bloom. J. Geophys.
534 Res. Oceans, 124(4), 2501-2512, https://doi.org/10.1029/2018JC014887, 2019.
535 Ricciardulli, L., Wentz, F.J., Smith, D.K.: Remote Sensing Systems QuikSCAT Ku-2011 [Daily]
536 Ocean Vector Winds on 0.25 deg grid, Version 4. Remote Sensing Systems, Santa Rosa, CA.
537 Available online at www.remss.com/missions/qscat, [Accessed 12 June 2022], 2011.
538 Wentz, F.J., Ricciardulli, L., Gentemann, C., Meissner, T., Hilburn, K.A., Scott, J..: Remote Se-
539 nsing Systems Coriolis WindSat [Daily] Environmental Suite on 0.25 deg grid, Version 7.0.
540 1. Remote Sensing Systems, Santa Rosa, CA. Available online at www.remss.com/missions
541 /windsat, [Accessed 12 June 2022], 2013.
542 Yang, H., Choi, J., Park, Y., Han, H., and Ryu, J.: Application of the Geostationary Ocean Color
543 Imager (GOCI) to estimates of ocean surface currents. J. Geophys. Res. Oceans, 119(6),
544 3988-4000, https://doi.org/10.1002/2014JC009981, 2014.